Open access • Journal Article • DOI:10.2514/2.3750

X-33 Hypersonic Boundary-Layer Transition — Source link

Scott A. Berry, Thomas J. Horvath, Brian R. Hollis, Richard A. Thompson ...+1 more authors

Institutions: Langley Research Center

Published on: 01 Sep 2001 - Journal of Spacecraft and Rockets (American Institute of Aeronautics and Astronautics (AIAA))

Topics: Boundary layer, Boundary layer thickness, Boundary layer control, Hypersonic speed and Surface roughness

AIAA 99-3560

X-33 HYPERSONIC BOUNDARY LAYER TRANSITION

Scott A. Berry, Thomas J. Horvath, Brian R. Hollis,
Richard A. Thompson, and H. Harris Hamilton II

NASA Langley Research Center,
Hampton, VA 23681

33rd AIAA Thermophysics Conference

June 28 - July 1, 1999 / Norfolk, VA

X-33 HYPERSONIC BOUNDARY LAYER TRANSITION

Scott A. Berry*, Thomas J. Horvath*, Brian R. Hollis*†, Rick A. Thompson, and H. Harris Hamilton II*†

Abstract

Boundary layer and aeroheating characteristics of several X-33 configurations have been experimentally examined in the Langley 20-Inch Mach 6 Air Tunnel. Global surface heat transfer distributions, surface streamline patterns, and shock shapes were measured on 0.013-scale models at Mach 6 in air. Parametric variations include angles-of-attack of 20-deg, 30-deg, and 40-deg; Reynolds numbers based on model length of 0.9 to 6.6 million; and body-flap deflections of 0, 10 and 20-deg. The effects of discrete and distributed roughness elements on boundary layer transition, which included trip height, size, location, and distribution, both on and off the windward centerline, were investigated. The discrete roughness results on centerline were used to provide a transition correlation for the X-33 flight vehicle that was applicable across the range of reentry angles of attack. The attachment line discrete roughness results were shown to be consistent with the centerline results, as no increased sensitivity to roughness along the attachment line was identified. The effect of bowed panels was qualitatively shown to be less effective than the discrete trips; however, the distributed nature of the bowed panels affected a larger percent of the aft-body windward surface than a single discrete trip.

*†Nomenclature

M	Mach number
M_e	Mach number at edge of boundary layer
Re	unit Reynolds number (1/ft)
Re_L	Reynolds number based on body length
Re_θ	momentum thickness Reynolds number
α	model angle of attack (deg)
δ	boundary layer thickness (in)
x	longitudinal distance from the nose (in)
y	lateral distance from the centerline (in)
L	reference length of model (10.00 in)
h	heat transfer coefficient (lbm/ft^2-sec), $=q/(H_{aw} - H_w)$ where $H_{aw} = H_{t2}$
h_{FR}	reference coefficient using Fay-Riddell calculation to stagnation point of a scaled sphere
q	heat transfer rate (BTU/ft^2-sec)
H	enthalpy (BTU/lbm)
k	roughness element height (in)
W	roughness element width (in)

Introduction

The Access to Space Study[1] by NASA recommended the development of a heavy-lift fully reusable launch vehicle (RLV)[2,3] to provide a next-generation launch capability to serve National space transportation needs at greatly reduced cost. This led to the RLV technology program, a cooperative agreement between NASA and industry. The goal of the RLV technology program is to enable significant reductions in the cost of access to space, and to promote the creation and delivery of new space services and other activities that will improve U.S. economic competitiveness. The program implements the National Space Transportation Policy, which is designed to accelerate the development of new launch technologies and concepts to contribute to the continuing commercialization of the national space launch industry. As part of the Single-Stage-To-Orbit (SSTO) RLV program, the X-33 was developed as a technology demonstrator. The X-33 Program will demonstrate the key design and operational aspects of a SSTO RLV rocket system so as to reduce the risk to the private sector in developing such a commercially viable system. The objective of NASA's technology development and demonstration effort, as stated in the National Space Transportation Policy is to support government and private sector decisions on development of an operational next-generation reusable launch system by the end of this decade. In order to meet its objectives, the X-33 program is an aggressive, focused launch technology development program, with extremely demanding technical objectives and milestones. A Cooperative Agreement is used between NASA and the industry partner, Lockheed Martin Skunkworks, to describe the responsibilities and milestones of both NASA and Lockheed. The X-33 is a slab-delta lifting body design with symmetric canted fins, twin vertical tails, and two outboard body flaps located at the rear of the fuselage. A linear aero-spike engine (Ref 4) is used to power the X-33, which is roughly a half-scale prototype of Lockheed's RLV design, the VentureStar. Figure 1 provides a comparison of the X-33 to the VentureStar and the Space Shuttle Orbiter.

* Aerospace Technologist, Aerothermodynamics Branch, Aero- and Gas-Dynamics Division, NASA Langley Research Center, Hampton, VA 23681.

† Member AIAA.

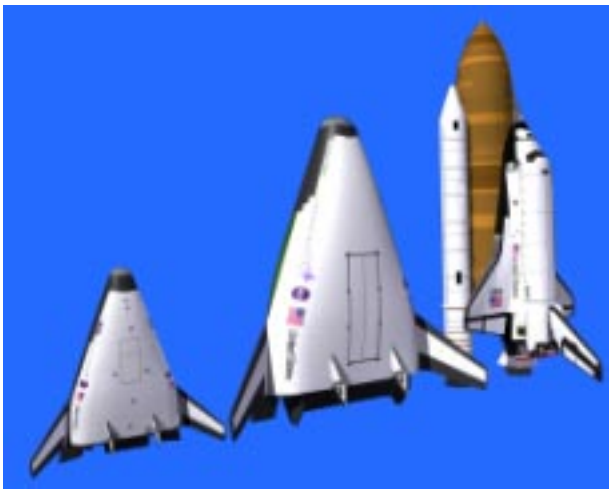

Figure 1 Comparison of X-33 to proposed RLV and the Space Shuttle.

As part of the Cooperative Agreement, NASA Langley Research Center (LaRC) has been tasked with providing experimental boundary layer transition and aeroheating data in support of X-33 aerothermodynamic development and design. To satisfy the objectives outlined in the task agreements, a combined experimental and computational approach was utilized. Results from early wind tunnel heating measurements were compared to laminar and turbulent predictions (Ref. 5). Preliminary results associated with the effort to characterize the boundary layer on the X-33 in flight were reported in Ref. 6. Since the time of these publications, additional tests have been completed which supplemented the original database and accommodated design changes to the vehicle shape. The most current experimental and computational aeroheating results are presented in this report and two companion papers (Refs. 7 and 8).

This report presents an overview of the results to date of the investigation into boundary layer transition for the X-33 configuration in NASA Langley Research Center (LaRC) facilities. The purpose of this investigation was to experimentally examine issues affecting boundary layer transition and the effect of transition on the aeroheating characteristics of the X-33. Over a series of wind tunnel entries in the LaRC 20-Inch Mach 6 Tunnel, the smooth body transition patterns, the effect of discrete roughness on and off windward centerline, and the effect of distributed bowed panels have been examined. The primary test technique that was utilized during these tests was the thermographic phosphor technique[9], which provides global surface heating images that can be used to assess the state of the boundary layer. Flow visualization techniques, in the form of oil-flow to provide surface streamline information and schlieren to provide shock system details were also used to supplement the heating data. Parametrics included in these tests were the effect of angle of attack (α of 20-deg, 30-deg, and 40-deg), unit Reynolds number (Re between 1 and 8 million/ft), body flap deflections (δ_{BF} of 0-deg, 10-deg, and 20-deg), and roughness. The roughness tests included both discrete and distributed trip mechanisms. The discrete roughness parametrics (which included height, size, and location) were included in these tests to provide information to develop roughness transition correlation for the X-33 vehicle and included results from both the centerline and attachment lines of the X-33. The distributed roughness was in the form of a wavy-wall that simulates the expected metallic TPS Panel bowing in flight due to temperature gradients across the panel.

Boundary Layer Transition in Flight

From the perspective of boundary layer transition, the X-33 has many similarities to the Space Shuttle Orbiter. Upon descent, both vehicles fly at angles of attack near 40-deg, which results in a moderately blunt flowfield that produces similar boundary layer edge conditions on the windward surface (M_e between 1.5 to 2.0). The Thermal Protection System (TPS) tiles that protect the windward surface are laid out in a diamond pattern similar to the Shuttle (see Fig. 2). The knowledge gained from the flight experience of the Shuttle forms the starting point with which to assess transition for the proposed X-33 flights.

The Shuttle Orbiters have flown numerous reentries into the earth's atmosphere. For a majority of these flights, boundary layer transition has been dominated by surface roughness (Ref. 10), in the form of launch-induced damage and/or protruding gap fillers. The random nature of this roughness allows for a wide range of free-stream conditions for the onset of transition: Mach numbers between 6 and 18 and length Reynolds numbers between 2.5 and 13 million. This amount of scatter does little to induce confidence with regard to reliable prediction of hypersonic boundary layer transition for future reentry vehicles.

Early in the Shuttle program the ceramic TPS was recognized to be relatively fragile and studies were per-

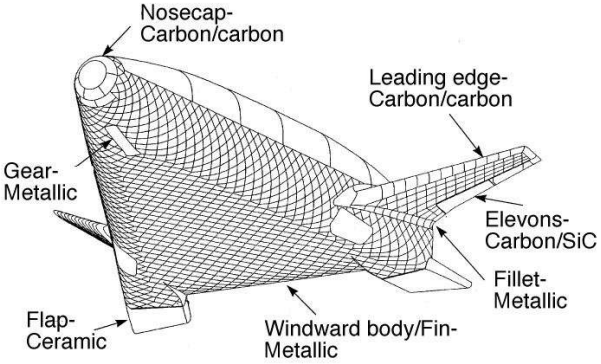

Figure 2 X-33 windward surface TPS.

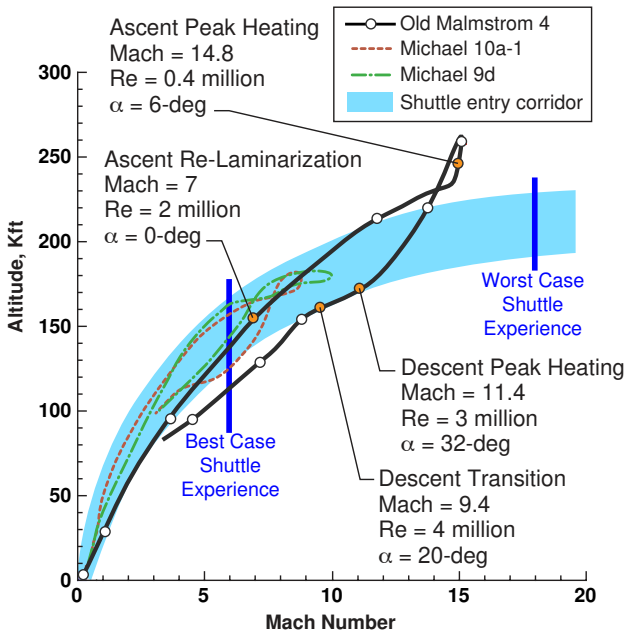

Figure 3 Malmstrom-4 (Old) trajectory.

formed to suggest alternatives which offer more durability and operability without sacrificing weight (Ref. 11). During these studies, a metallic TPS was identified as the lightest system to provide a significant improvement in durability and operability for the shuttle program, but was never implemented. A derivative of this metallic TPS has been selected for use on the windward surface of the X-33 (Refs. 12 and 13), as shown in Fig. 2. This system is expected to offer improved durability against the random surface defects that continue to plague the Shuttle. However, a detriment of this system is that it provides an additional type of surface roughness that has received very little attention over the years. During a hypersonic entry, thermal gradients within the metallic TPS panels will produce an outward bowing of the panels on the order of 0.25-in. The effect of this panel bowing on hypersonic boundary layer transition is largely unknown and is part of the current investigation that will be described in this paper.

The sub-orbital trajectory used for the design of the TPS is shown in Fig. 3 and is designated as Old Malmstrom-4. This is a high Mach number trajectory that would land the X-33 at Malmstrom Air Force Base in Montana. The initial flights of the X-33 are lower Mach number trajectories to Michaels Air Force Base in Utah (preliminary Michaels trajectories are also shown for comparison). Some select points (relevant to the TPS design) along the Old Malmstrom-4 trajectory are illustrated in Fig. 3. On ascent the X-33 windward surface is assumed, for the purpose of the TPS design, to remain turbulent until Re_L = 2 million. Thus, during peak heating on ascent, the windside boundary layer will be laminar and the vehicle will be at a low angle of attack. As the top of the trajectory is reached, the vehicle pitches up to high angles of attack for most of the hypersonic descent. A second peak heating point occurs on descent at a Mach number near 11. Based on earlier results published in Ref. 6, the X-33 boundary layer is expected to transition back to a turbulent state at a Mach number near 9. However, when viewed against the varied results experienced on the Shuttle, also shown in Fig. 3, the need to minimize known transition by-pass mechanisms, which could force earlier transition (prior to the descent peak heating point), is evident.

Transition Prediction Approach

A series of wind tunnel tests (see Table 1) were performed to investigate the X-33 aeroheating and boundary layer characteristics, while tracking changes to the configuration. Over 1100 tunnel runs from 16 entries in two facilities have been completed on four X-33 configurations since Aug 1996. The evolution of the X-33 configuration from the onset of Phase II has necessitated multiple entries into LaRC facilities to investigate the effects of outer mold line (OML) changes to X-33's aeroheating environment. The OML for the X-33 started with the original D-Loft concept, then the F-Loft Revision C (Rev-C), the F-Loft Revision F (Rev-F), and finally the F-Loft Revision G (Rev-G). These four configurations have been tested in LaRC facilities for both baseline aeroheating data (i.e. wide ranges of angle of attack, yaw, Reynolds number, body flap deflection, etc.), and to investigate the effects of surface roughness (both discrete and distributed), and test technique (model scale, blade vs. sting support, etc.). The D-loft configuration emerged from the end of the Phase I competition and was heavily tested in the early part of Phase II. The Rev-C configuration instituted small modifications to the nose shape (to simplify the construction of the metallic TPS panels) and to the base region (in the vicinity of the engine). The Rev-F has the same forebody shape as Rev-C, but the dihedral of the canted fins was lowered from 37-deg to 20-deg (to improve pitch-trim characteristics across the speed range) and the size of the body flaps and vertical tails was increased. Finally the Rev-G had some minor modifications to the leeside and canted-fin fillet. Additional details regarding the OML changes can be found in Ref. 7.

The testing sequence and model configurations tested are listed in Table 1. First, the effect of discrete roughness elements on the centerline of the D-Loft forebody was investigated in test 6737. Then during test 6763, the effect of discrete roughness on the centerline of the Rev-F configuration was investigated. These tests utilized the same approach that was used during an investigation into discrete roughness elements on the Shuttle Orbiter (Ref. 14) that has shown good agreement

with flight data (Ref. 15). These early test results were presented in Ref. 6. The effect of distributed roughness in the form of a wavy-wall surface (simulating bowed metallic thermal protection system tiles) on Rev-F was investigated in test 6769. The windward attachment line was examined during test 6770 for comparison to trends found on the centerline. These results are detailed in Ref. 16. And finally, extended bowed panels on Rev-G were investigated during test 6786. Collectively, these tests provide a systematic investigation of several different boundary layer trip mechanisms while tracking the OML changes of the X-33 vehicle.

Experimental Methods

Test Facility

The present experiments were conducted in the LaRC 20-Inch Mach 6 Air Tunnel. Miller (Ref. 17) provides a detailed description of this hypersonic blow-down facility, which uses heated, dried, and filtered air as the test gas. Typical operating conditions for the tunnel are stagnation pressures ranging from 30 to 500 psia, stagnation temperatures from 760 to 940-degR, and freestream unit Reynolds numbers from 0.5 to 8 million per foot. A two-dimensional, contoured nozzle is used to provide nominal freestream Mach numbers from 5.8 to 6.1. The test section is 20.5 by 20 inches; the nozzle throat is 0.399 by 20.5-inch. A bottom-mounted model injection system can insert models from a sheltered position to the tunnel centerline in less than 0.5-sec. Run times up to 15 minutes are possible with this facility, although for the current heat transfer and flow visualization tests, the model was exposed to the flow for only a few seconds. Flow conditions were determined from the measured reservoir pressure and temperature and the measured pitot pressure at the test section.

Test Techniques

Surface Heating

The rapid advances in image processing technology which have occurred in recent years have made digital optical measurement techniques practical in the wind tunnel. One such optical acquisition method is two-color relative-intensity phosphor thermography, which is currently being applied to aeroheating tests in the hypersonic wind tunnels of NASA LaRC. Details of the phosphor thermography technique are provided in Refs. 9, 18, and 19, while Refs. 6, 14, 20, and 21 are recent examples of the application of the technique to wind tunnel testing. With this technique, ceramic wind tunnel models are fabricated and coated with phosphors that fluoresce in two regions of the visible spectrum when illuminated with ultraviolet light. The fluorescence intensity is dependent upon the amount of incident ultraviolet light and the local surface temperature of the phosphors. By acquiring fluorescence intensity images with a color video camera of an illuminated phosphor model exposed to flow in a wind tunnel, surface temperature mappings can be calculated on the portions of the model that are in the field of view of the camera. A temperature calibration of the system conducted prior to the study provides the look-up tables that are used to convert the ratio of the green and red intensity images to global temperature mappings. With temperature images acquired at different times in a wind tunnel run, global heat transfer images are computed assuming one-dimensional heat conduction. The primary advantage of this technique is the global resolution of the quantitative heat transfer data. Such data can be used to identify the heating footprint of complex, three-dimensional flow phenomena (e.g., transition fronts, turbulent wedges, boundary layer vortices, etc.) that are extremely difficult to resolve by discrete measurement techniques. Phosphor thermography is routinely used in Langley's hypersonic facilities as quantitative global surface heating information is obtained from models that can be fabricated quickly (within a few weeks) and economically (cost an order of magnitude less than the thin-film technique). Recent comparisons of heat transfer measurements obtained from phosphor thermography to conventional thin-film resistance gauges measurements (Ref. 22) and CFD predictions (Ref. 5, 6, 20, and 23) have shown excellent agreement.

Flow Visualization

Flow visualization techniques, in the form of schlieren and oil-flow, were used to complement the surface heating tests. The LaRC 20-Inch Mach 6 Air Tunnel is equipped with a pulsed white-light, Z-pattern, single-pass schlieren system with a field of view encompassing the entire 20-in test core. Surface streamline patterns were obtained using the oil-flow technique. Both schlieren and oil-flow images were recorded with a high-resolution digital camera.

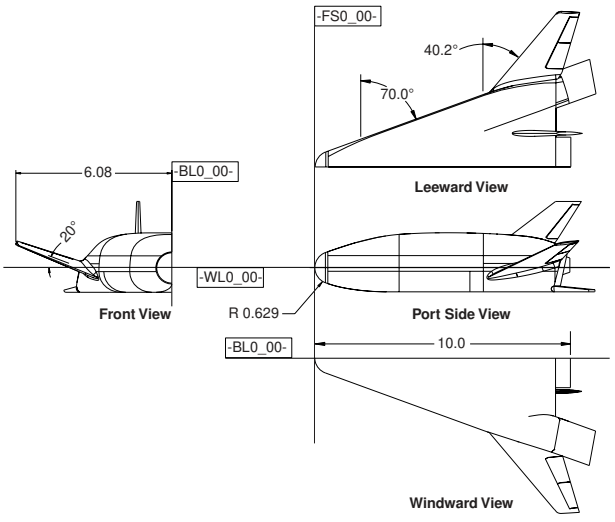

Figure 4 X-33 Rev-F Configuration.

Figure 5 Photograph of X-33 Rev-F models with various flap deflections.

Model Description

The X-33 Rev-F model dimensions are shown in Fig. 4. A rapid prototyping technique was used to build resin stereolithography (SLA) models with various, detachable body flaps on both the port and starboard region of the base of the vehicle. The SLA model was then used with the various body flaps as a pattern to cast several ceramic model configurations. Figure 5 is a photograph of three Rev-F models that were cast with the various flap deflections. Additional details about the various model configurations that were tested can be found in Ref. 16.

In order to obtain accurate heat transfer data using the one-dimensional heat conduction equation, models need to be made of a material with low thermal diffusivity and well-defined, uniform, isotropic thermal properties. Also, the models must be durable for repeated use in the wind tunnel and not deform when thermally cycled. To meet these requirements, a unique, silica ceramic investment slip casting method has been developed and patented (Ref. 24). A hydraulically setting magnesia ceramic was used to backfill the ceramic shell, thus providing strength and support to the sting structure. The models were then coated with a mixture of phosphors suspended in a silica-based colloidal binder.

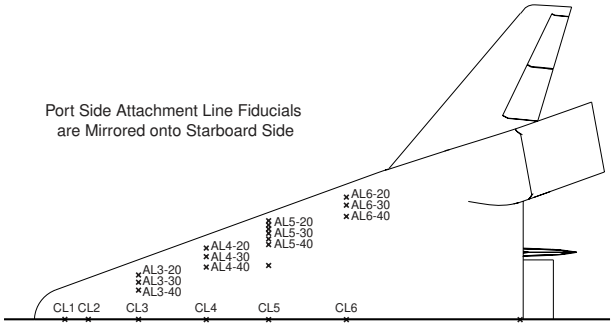

Figure 6 Sketch of trip locations and fiducial marks.

This coating consisted of a 5:1 mixture of lanthanum oxysulfide (La_2O_2S) doped with trivalent europium and zinc cadmium sulfide (ZnCdS) doped with silver and nickel in a proprietary ratio. The coatings typically do not require refurbishment between runs in the wind tunnel and have been measured to be approximately 0.001 inches thick. The final step in the fabrication process is to apply fiducial marks along the body to assist in determining spatial locations accurately. The fiducial marks used for the present study are shown in Fig. 6 and the non-dimensional locations are listed in Table 2.

The roughness elements used in this study were similar to those used in Refs. 6 and 14, which were fabricated to simulate a raised Thermal Protection System (TPS) tile and were cut from 0.0025-inch thick Kapton tape. Presented in Fig. 7 is a sketch of a typical discrete trip showing dimensions and orientation. Variations on the roughness heights (k) were obtained by stacking multiple layers of Kapton tape (k = 0.0025, 0.0050, and 0.0075-inch). Roughness elements fabricated from Kapton tape were applied to the various locations of interest on the model and could be easily removed without adversely affecting the phosphor coating. Kapton tape was chosen through a trial and error process based on the ease of fabrication and application of the roughness elements, as well as the durability of the material (and adhesive) to heat and shear stress loading. The simulated tile roughness elements were placed directly over the various fiducial marks, which were previously located on the model.

Bowed-panel models were also tested to simulate the effect of the wavy-wall windward surface that would be produced by the temperature gradients within the metallic TPS panels. The five configurations tested are shown in Fig. 8. Each configuration was constructed with nominal bow heights of 0.002, 0.004, 0.006, and

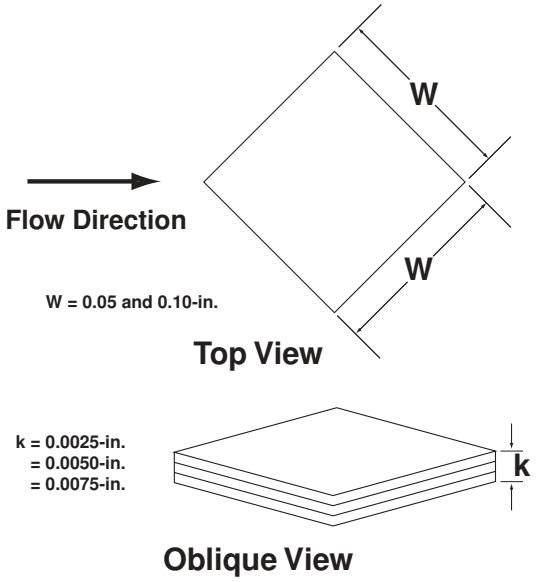

Figure 7 Sketch of trips showing orientation, width, and height.

0.008-in. Two models of each configuration was built and tested to provide a statistical database with which to assess the results.

Test Conditions

The LaRC 20-Inch Mach 6 Air Tunnel provides a freestream unit Reynolds number variation of 0.5 to 8.0 million per foot. For a 0.0132-scale model, this corresponds to a length Reynolds number of approximately 0.41 to 6.7 million. For the baseline data, the model angle of attack (α) was varied from 20-deg to 40-deg in 10-deg increments and the sideslip was maintained at zero for all the runs presented herein. For each model configuration, the unit Reynolds number was varied between 1 and 8 million per foot to obtain the smooth baseline data for comparison to the tripped data. For the transition testing, the same *Re* range with the roughness element firmly applied to the location of interest in order to determine the incipient, critical, and effective Reynolds numbers (using the vernacular coined by Bertin[25]). The maximum Reynolds number at which laminar flow was maintained behind the trip identifies the incipient value. The Reynolds number where significant nonlaminar flow first appears downstream of the roughness element identifies the critical value. And the minimum Reynolds number where the transition front is fixed at the roughness element identifies the effective value.

Data Reduction

Heating rates were calculated from the global surface temperature measurements using one-dimensional semi-infinite solid heat-conduction equations, as discussed in detail in Refs. 9 and 19. Based on considerations presented in Ref. 9, phosphor system measurement error is believed to be better than ±8%, with overall experimental uncertainty of ±15%. Heating distributions are presented in terms of the ratio of heat-transfer coefficient h/h_{FR}, where h_{FR} corresponds to the Fay and Riddell[26] stagnation-point heating to a sphere with radius 0.629-in (the nose radius of the Rev-F configuration scaled to the model size). Repeatability of the centerline heat transfer distributions was found to be generally better than ±4%.

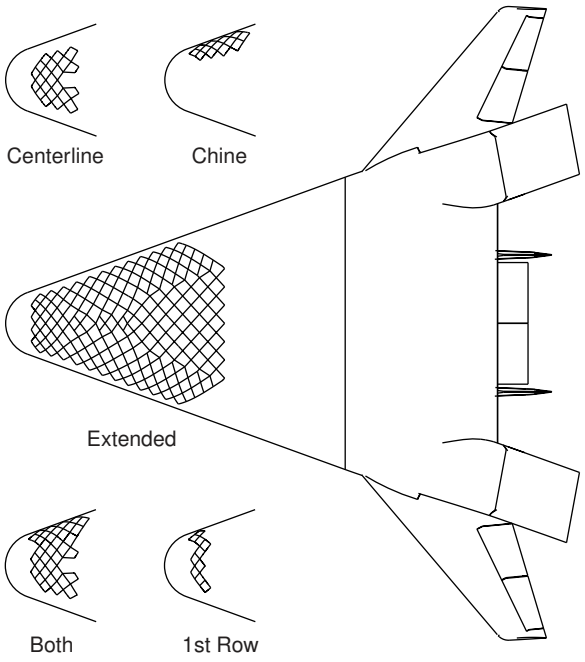

Figure 8 Sketch of various bowed-panel configurations.

Computational Methods

Computational predictions for comparison to the wind tunnel aeroheating test results were generated at select angles-of-attack and test conditions using the General Aerodynamic Simulation Program (GASP) code,[27] and the Langley Approximate Three-Dimensional Heating Analysis (LATCH) code.[28] The GASP computations were used to assess the state of the boundary layer for the wind tunnel cases, while the LATCH results were used to generate the boundary layer transition correlation parameters. GASP is a three–dimensional, finite-volume Navier-Stokes solver that incorporates numerous options for flux-splitting methods, thermochemical and turbulence models, and time-integration schemes. A perfect gas air model was employed and both fully laminar and fully turbulent solutions were obtained. Further details regarding the GASP computations can be found in Ref. 8. The LATCH code is an approximate three-dimensional heating code based on the axisymmetric analog for general three-dimensional boundary layers. An integral heating method is used to compute the heating rates along three-dimensional inviscid streamlines. The inviscid streamlines were supplied using an inviscid version of the Langley Aerothermodynamic Upwind Relaxation Algorithm (LAURA) code. Further details regarding the LATCH computations can be found in Ref. 5.

Discussion of Results

Smooth Body

The effect of angle of attack on smooth-body boundary layer transition is shown in Fig. 9. These heating images were obtained on a Rev-F model with a body flap deflection (δ_{BF}) of 20-deg for a unit Reynolds number (*Re*) of approximately 8 million per foot. As will be discussed in more detail subsequently, the increased heating region towards the aft-end of the model identifies the onset of boundary layer transition. Note the changing shape of the transition front as α increases. Figure 9a (α = 20-deg) shows two transition lobes separated by a laminar region on centerline. At α = 30-deg (Fig. 9b) the two lobes have begun to merge on centerline. For α = 40-deg (Fig. 9c) a single parabolic transition front symmetric about the centerline appears. This behavior was first noted in Ref. 6 on an early X-33 con-

figuration and appears to be related to changes in the direction of the forebody streamlines, as reported in Ref. 7. At the lower angles of attack the forebody generates surface streamlines which curve predominately in towards the centerline (inflow). This promotes a thickening of the boundary layer on centerline that tends to delay transition. The highly curved streamlines on the outboard regions of the forebody would likely induce crossflow instabilities that feed in from the chines. At the higher angles of attack, the surface streamlines tend to straighten out or even reverse direction to a slight outflow condition. For these cases, boundary layer transition along the forebody centerline is likely to be dominated by the flow from the nose region.

The effect of varying Reynolds number on extracted heat transfer profiles along the model centerline for each α is shown in Fig. 10 with comparison of the smooth body results to tripped cases and to laminar and turbulent heating predictions from Ref. 8. For the smooth body data, the heating profiles are seen to agree (within the experimental uncertainty) with the laminar GASP predictions until the onset of natural transition occurs on the aft-end of the model at higher Reynolds numbers. The forward progression of the transition onset point with increasing Re is the furthest forward at α = 40-deg (Fig 10c). The tripped cases were selected for comparison with the turbulent predictions and are also observed to agree within the experimental uncertainty. The LATCH results do not compare as favorably along the centerline; however, as shown in Ref. 8, this disparity is only along the centerline as off-centerline the results compare within the experimental uncertainty.

Discrete Roughness along Model Centerline

As an example of the many discrete trip results that were obtained, the effect of a 0.005-in discrete trip at location CL3 is shown in Fig. 11 for each α. These heating images were obtained on a Rev-F model with a δ_{BF} of 0-deg. Figure 11a illustrates that for α = 20-deg and $Re = 4.2\text{x}10^6$/ft, the 0.005-in trip at CL3 just begins to have an effect on the downstream boundary layer. As the turbulent wedge does not start immediately behind the trip, this case would be classified as "critical." For α = 30-deg and $Re = 4.2\text{x}10^6$/ft (Fig. 11b), the trip now produces a turbulent wedge directly behind the trip. This case would be classified as "effective." As the angle of attack is increased to 40-deg (Fig. 11c), the trip is now an "effective" trip at $Re = 3.1\text{x}10^6$/ft.

From the sample results presented in Fig. 11, one might be tempted to conclude that the X-33 vehicle would be more sensitive to discrete trips at higher angles of attack. This conclusion is not supported when all the results for discrete trips are used, in conjunction with the boundary layer calculations, to generate a Re_θ/M_e vs. k/δ correlation. Figure 12 provides the results of this correlation for all the discrete trip results along the model centerline for angles of attack of 20, 30, and 40-deg as reported in Ref. 6. The simple relations shown conservatively approximate the well-behaved patterns of incipient and effective transition data. While the LATCH heating calculations are not in close agreement with the experimental results along the centerline, the effect of this over-prediction should not strongly affect the boundary layer edge parameters used for the present correlation. Ref. 14 reported a similar disagreement with comparison to heating predictions which resulted in only a 1 to 2% error in boundary layer edge calculations.

The experimental transition results presented thus far have already supported the X-33 program. As discussed in Ref. 6, a value of Re_θ/M_e = 250 at x/L = 0.8 on the windward centerline was chosen as the transition criterion based on a conservative view of the smooth body and discrete centerline roughness results, as well as experience from the Shuttle. The simplicity of this result has allowed development of a numerical tool that predicts when transition will occur on the windward centerline for a given altitude, velocity, and angle of attack condition. Coupling this tool with trajectory simulations enable modifications of the flight profile to be made to ensure TPS design constraints are not exceeded. The transition tool is based on a database of numerical simulations that cover the range of altitudes, velocities, and angles of attack expected in flight. Further details regarding the development and utility of this transition function can be found in Ref. 6. Figure 13 illustrates the function in relation to the TPS-design trajectory. Also, the discrete roughness data has been used to estimate the allowable roughness heights for the flight vehicle, as shown in Fig. 14. Using the flight criterion for transition onset (Re_θ/M_e = 250) and the relations from Fig. 12, an allowable k/δ of 0.2 is located. Using this value of k/δ and the calculated boundary layer thickness at the point on the trajectory that corresponds to the onset of transition, the allowable roughness heights over the windward surface are inferred.

Discrete Roughness Off-Centerline

Once the roughness criterion was established for the X-33 centerline, the next step was to verify if the discrete centerline criterion was applicable to off-centerline locations as well. The attachment line has been suggested by some to be one of the most important off-centerline locations for increased sensitivity to surface roughness (Ref 29). A program was initiated to investigate the effect of disturbances along the attachment lines for the X-33. The LATCH code (Ref. 5) was used to predict the location of the attachment lines for angles of attack of 20, 30, and 40-deg (with nominal tunnel flow conditions as inputs). These attachment lines were used to locate the fiducial marks on the model for placement

of the individual roughness elements (note that the attachment line fiducials correspond in terms of x/L to the same centerline locations used for the previous discussion). These fiducial mark locations are shown in Fig. 6. Both the port and starboard side of the windward surface was marked in order to examine flow symmetry. The experimental attachment lines were determined using the oil-flow technique and were found to correspond to prediction. For example, in Fig. 15, the attachment line is found by locating the surface streamline that neither curves to the leeside nor towards the centerline, and can be seen for this 30-deg example to coincide with the middle fiducial marks (α = 30-deg). Similar results were obtained for angles of attack of 20 and 40-deg.

Once the attachment line locations were verified for each angle of attack, the roughness effects were examined. Examples of typical heating images, which illustrate flow symmetry, and extracted heating profiles along the attachment line are provided in Figs. 16 and 17. For α = 30-deg (Fig. 16), 0.005-in trips at station 4 (on the port and starboard attachment lines, as well as the centerline) appear to be effective at $Re = 3.1 \times 10^6$/ft on the attachment lines, but not along the centerline. Similar results are shown in Fig. 17 for α = 40-deg. Again, one might be tempted to draw the conclusion from these images that attachment lines appear to be more sensitive to discrete trips than the centerline. However, this conclusion is also not supported when the attachment line discrete trip results are compared to the results for the centerline discrete trip correlation (Fig. 12). This comparison is shown in Fig. 18 (a few data points have been omitted for clarity). The diagonal lines correspond to each Reynolds number sweep for a given trip configuration. At low Re there is no effect of the trip (open circle for laminar); as Re increases the first effects are noticed (open square for transitional); and finally fully turbulent conditions up to the trip (filled square). In general, these off-centerline results show very good agreement with the previous centerline data. Thus, the transition correlation that was published earlier for the centerline data[6] has now been shown to be applicable to off-centerline locations as well. This study did not show any evidence of a higher sensitivity to roughness elements placed along the attachment line. However, the images of Figs. 16 and 17 illustrate that disturbances along the attachment lines will have a bigger impact on the aft-body than trips on centerline.

Poll (Ref. 29) has proposed a transition onset criterion for attachment line boundary layer transition. In an effort to compare Poll's criterion with the current discrete roughness results, data from Poll's swept cylinder attachment-line curve (for incompressible flow) has been recast in terms of the current X-33 results. As discussed previously, the LATCH code has been used to compute heating and boundary layer edge parameters on the X-33 vehicle. Hollis, et al. (Ref. 8) has shown that the LATCH computations are in very good agreement with Navier-Stokes calculations in the chine region where the attachment lines are located. Using the LATCH code, the momentum thickness Reynolds number can be computed on the attachment line along with other boundary layer edge properties. This information can then be used as input to a swept cylinder boundary layer code (Ref. 30) to compute the momentum thickness Reynolds number for an "equivalent" swept cylinder. The only unknown in this computation is the velocity gradient normal to the attachment line. By iterating on this velocity gradient, the momentum thickness Reynolds number from the swept cylinder calculation can be matched to the approximate three-dimensional momentum thickness Reynolds computed by LATCH. This yields an equivalent velocity gradient on the attachment line, which is required to compute Poll's transition parameter (Ref. 29). Using this approach, Poll's attachment line criterion (Fig 2. in Ref. 29) can be recast in terms of the discrete roughness parameters for the X-33, as is shown in Fig. 19. Presented in this manner, the original Poll attachment-line criterion for transition onset appears less conservative than the current incipient curve developed for X-33 (solid line in Fig 19).

Distributed Roughness

The final transition issue that was investigated for the X-33 was the effect of the bowed metallic TPS panels. Five configurations were selected for testing which placed the location and extent of the bowed panels at various stations on the windward forebody, as shown in Fig. 8. The maximum bow height over the windward surface in flight is expected to be on the order of 0.15 to 0.30-in. Based on the scale of the model (1.32%), this corresponds to geometrically scaled bow heights on the order of 0.002 to 0.004-in. Additional heights of 0.006 and 0.008-in were also selected to provide an adequate range of wall waviness. For all configurations and heights, a primary and secondary model was built and tested to provide repeatability data.

The series of tests on the various bowed panel configurations has only recently been completed. Adequate time to fully analyze this data has not been available. As such, the results shown here will be mostly of a qualitative nature, in the form of heating and flow visualization images. A photograph of the 0.008-in Extended bowed panels model is shown in Fig. 20. An example of the effect of this worst-case bowed-panels model on the surface streamlines for α = 40-deg and $Re = 2 \times 10^6$/ft is shown in Fig. 21. The surface streamlines are seen to serpentine around the various bowed panels. The corresponding schlieren image, shown in Fig. 22, indicates that this level of bowing is sufficient enough to generate a series of shocklets that are seen to reflect

off the bow shock. Not surprisingly, this amount of disturbance to the flow field is enough to affect the boundary layer, as shown in the corresponding heating image of Fig. 23.

The example selected is an extreme case that has over twice as much bowing geometrically than is expected in flight. However, the forward movement of transition for this extreme case can be seen to be still less than the effective discrete trip case shown in Fig 11c, which corresponds to a smaller disturbance at a lower Reynolds number. To illustrate this point further, Fig. 24 is a simplified comparison of the X-33 flight criterion as applied to the wind tunnel transition to the transition onset results for smooth, discrete, and bowed-panels. The three curves representing each α correspond to the calculated Re_θ/M_e at the centerline $x/L = 0.8$ location as a function of the tunnel Re range. The onset of transition results (at $x/L = 0.8$) for the smooth, discrete, and bowed-panels data for each α was located along these three curves. The flight criterion of $Re_\theta/M_e = 250$ is shown to conservatively cover the smooth model transition onset results for all reentry α. Also, the bowed panel results are also mostly covered by the built-in conservatism. On the other hand, the discrete results are shown to be more effective than the bowed panels at forcing transition onset at $x/L = 0.8$. Further analysis of the distributed bowed panel results is required to determine if bowed panels in the vicinity of the chine region might influence the crossflow dominated flow field at lower angles of attack.

Concluding Remarks

A series of experimental investigations into several issues affecting boundary layer transition on the X-33 vehicle has been performed in the LaRC 20-Inch Mach 6 Tunnel. These investigations examined natural transition on a smooth body, transition due to discrete roughness on the centerline and attachment lines, and transition due to distributed roughness in the form of "wavy-wall" bowed panels. Phosphor thermography was used to provide global heating images of the windward surface and assess the state of the boundary layer. The size and location of the various roughness mechanisms were systematically altered and the subsequent response of the boundary layer was captured in the surface heating images. The experimental heating levels were compared to predictions to determine the onset location of transition and fully turbulent flow. Flow field parameters from a boundary layer code were used for analysis of transition correlations.

The smooth body results indicate a significant change in the transition pattern as the reentry angle of attack changes from 20-deg to 40-deg. At lower α, a two-lobed transition front, indicative of crossflow transition from the chine regions, is evident, while at higher α, a single parabolic transition front is centered about the model centerline. The discrete roughness results on centerline were used to provide a transition correlation for the X-33 flight vehicle that was applicable across the range of reentry angles of attack. To estimate the onset of transition in flight, the value of $Re_\theta/M_e = 250$ at $x/L = 0.8$ on the windward centerline was selected. This corresponded to a $k/\delta = 0.2$ from the discrete correlation curve, which was used to estimate the allowable roughness for the flight vehicle. The attachment line discrete roughness results were shown to be consistent with the centerline results, as no increased sensitivity to roughness along the attachment line was identified. However, the effective trips on the attachment lines were shown to affect a larger percent of the aft-body than trips on centerline. Finally, the effect of bowed panels was qualitatively shown to be less effective than the discrete trips, however, the distributed nature of the bowed panels affected a larger percent of the aft-body than a single discrete trip. Further analysis of the bowed panel results to analyze the off-centerline effects is required.

Acknowledgments

The following individuals were critical to the successful completion of this work: Mark Cagle, Joe Powers, Mark Griffin, Mike Powers, Rhonda Manis, Grace Gleason, Johnny Ellis, Bert Senter, Sheila Wright, Glenn Bittner, Steve Alter, Matt Kowalkowski, Derek Liechty, and Richard Wheless. The authors greatly appreciate their contributions.

References

1.Bekey, I., Powell, R., and Austin. R., "NASA Studies Access to Space," *Aerospace America*, May 1994, pp. 38-43.

2.Cook, S. A., "X-33 Reusable Launch Vehicle Structural Technologies," AIAA Paper 97-10873, Nov. 1996.

3.Freeman Jr., D. C., Talay, T. A., and Austin, R. E., "Reusable Launch Vehicle Technology Program," AIAA Paper IAF 96-V.4.01, Oct. 1996.

4.Baumgartner, R. I., and Elvin, J. D., "Lifting Body – An Innovative RLV Concept," AIAA Paper 95-3531, Sept. 1995.

5.Hamilton, H., Berry, S., Horvath, T., and Weilmuenster, J., "Computational/ Experimental Aeroheating Predictions for X-33 Phase II Vehicle," AIAA Paper 98-0869, January 1998.

6.Thompson. R. A., Hamilton, H. H., Berry, S. A., and Horvath, T. J., "Hypersonic Boundary Layer Transition for X-33 Phase II Vehicle," AIAA Paper 98-0867, January 1998.

7.Horvath, T. J., Berry, S. A., Hollis, B. R., Liechty, D. S., Hamilton, H. H. II, and Merski, N. R., "X-33 Experi-

mental Aeroheating at Mach 6 Using Phosphor Thermography," AIAA Paper 99-3558, June 1999.

8.Hollis, B. R., Horvath, T. J., Berry, S. A., Hamilton, H. H. II, and Alter, S. J., "X-33 Computational Aeroheating Predictions and Comparison with Experimental Data," AIAA Paper 99-3559, June 1999.

9.Merski, N. R., "Reduction and Analysis of Phosphor Thermography Data With the IHEAT Software Package," AIAA Paper 98-0712, Jan. 1998.

10.Bouslog, S. A., An, M. Y., and Derry, S. M., "Orbiter Windward Surface Boundary Layer Transition Flight Data," NASA CP 3248, Orbiter Experiments (OEX) Aerothermodynamics Symposium, April 1995.

11.Kelly, H. N., and Webb, G. L., "Assessment of Alternate Thermal Protection Systems for the Space Shuttle Orbiter," AIAA Paper 82-0899, June 1982.

12.Blosser, M. L., "Development of Metallic Thermal Protection Systems for the Reusable Launch Vehicle," NASA TM 110296, October 1996.

13.Bouslog, S. A., Moore, B., Lawson, I., and Sawyer, J. W., "X-33 Metallic TPS Tests in NASA-LaRC High Temperature Tunnel," AIAA Paper 99-1045, Jan. 1999.

14.Berry, S. A., Bouslog, S. A., Brauckmann, G. J., and Caram, J. M., "Shuttle Orbiter Experimental Boundary-Layer Transition Results with Isolated Roughness," *Journal of Spacecraft and Rockets*, Vol. 35, No. 3, 1998, pp. 241-248.

15.Caram, J. M., Private Communication, NASA JSC, Oct 1998.

16.Berry, S. A., Horvath, T. J., Kowalkowski, M. K., and Liechty, D. S., "X-33 (Rev-F) Aeroheating Results of Test 6770 in NASA Langley 20-Inch Mach 6 Tunnel," NASA/TM-1999-209122, March 1999.

17.Miller, C. G., "Langley Hypersonic Aerodynamic/Aerothermodynamic Testing Capabilities - Present and Future," AIAA Paper 90-1376, June 1990.

18.Buck, G. M., "Automated Thermal Mapping Techniques Using Chromatic Image Analysis," NASA TM 101554, April 1989.

19.Buck, G. M., "Surface Temperature/Heat Transfer Measurement Using A Quantitative Phosphor Thermography System," AIAA Paper 91-0064, Jan. 1991.

20.Berry, S. A., Horvath, T. J., DiFulvio, M., Glass, C., and Merski, N. R., "X-34 Experimental Aeroheating at Mach 6 and 10," AIAA Paper 98-0881, January 1998.

21.Horvath, T. J., Rhode, M. N., and Buck, G. M., "Aerothermodynamic Measurements on a Proposed Assured Crew Return Vehicle (ACRV) Lifting Body Configuration at Mach 6 and 10 in Air," AIAA Paper 90-1744, June 1990.

22.Micol, J. R., "Aerothermodynamic Measurement and Prediction for a Modified Orbiter at Mach 6 and 10 in Air," *Journal of Spacecraft and Rockets*, Vol. 32, No. 5, 1995, pp. 737-748.

23.Loomis, M. P., Venkatapathy, E., Davies, C. B., Campbell, C. H., Berry, S. A., Horvath, T. J., and Merski, N. R., "Aerothermal CFD Validation and Prediction for the X-38 Program," AIAA Paper 97-2484, June 1997.

24.Buck, G. M. and Vasquez, P., "An Investment Ceramic Slip-Casting Technique for Net-Form, Precision, Detailed Casting of Ceramic Models," U. S. Patent 5,266,252, November 30, 1993.

25.Bertin, J. J., Hayden, T. E., and Goodrich, W. D., "Shuttle Boundary-Layer Transition Due to Distributed Roughness and Surface Cooling," *Journal of Spacecraft and Rockets*, Vol. 19, No. 5, 1982, pp. 389-396.

26.Fay, J. A., and Riddell, F. R., "Theory of Stagnation Point Heat Transfer in Dissociated Air," *Journal of Aeronautical Sciences*, Vol. 25, No. 2, 1958.

27.Aerosoft, "GASP Version 3, The General Aerodynamic Simulation Program, Computational Flow Analysis Software for the Scientist and Engineer, User's Manual," Aerosoft Inc., Blacksburg, VA, May 1996.

28.Hamilton, H. H. II, Greene, F. A., DeJarnette, F. R., "Approximate Method for Calculating Heating Rates on Three-Dimensional Vehicles," *Journal of Spacecraft and Rockets*, Vol. 31, No. 3, 1994, pp. 345-354.

29.Poll, D. I. A., "A New Hypothesis for Transition on the Windward Face of the Space Shuttle," *Journal of Spacecraft and Rockets*, Vol. 23, No. 6, 1986, pp. 605-611.

30.Adams, J. C. Jr., and Martindale, W. R., "Hypersonic Lifting Body Windward Surface Flow-Field Analysis for High Angles of Incidence," AEDC-TR-73-2, Feb. 1993.

Table 1: X-33 Phase II Aeroheating Tests in NASA LaRC AB Tunnels

Year	Tunnel	Test	Occupancy Dates	Runs	Description
1996	20” M6	6731	Aug 28 - Sept	1-46	D-loft Forebody Baseline
1996	M6 CF4	114	Oct 17 - Nov 6	1-43	Yaw Dispersions
1996	20” M6	6737	Dec 6 - Dec 20	1-174	D-loft Forebody Transition
1997	20” M6	6751	June 23 - June 30	1-52	Generic Bowed Panel Models
1997	20” M6	6751	July 15 - July 17	52-56	Generic Bowed Panel Models
1997	20” M6	6753	July 17 - July 22	1-22	Rev C (37-deg Dihedral) Baseline
1997	20” M6	6753	Aug 12 - Aug 20	22-50	Rev C (37-deg Dihedral) Baseline
1997	20” M6	6751	Aug 27 - Aug 29	56-99	Generic Bowed Panel Models
1997	20” M6	6751	Sept 22 - Sept 24	100-115	Generic Bowed Panel Models
1997	20” M6	6763	Dec 30 - Jan 6	1-29	Rev F (20-deg Dihedral) Baseline
1998	20” M6	6763	Jan 15 - Jan 22	30-68	Rev F (20-deg Dihedral) Baseline
1998	20” M6	6763	Feb 17 - Mar 4	69-203	Rev F Discrete Roughness
1998	20” M6	6769	Apr 3 - Apr 17	1-123	Rev F Bowed Panels
1998	20” M6	6770	May 22 - Jun 24	1-185	Rev F Attach-Line Roughness
1998	20” M6	6777	Aug 5 - Aug 12	1-40	Rev F Blade vs. sting
1999	20” M6	6786	May 3 - May 14	1-84	Rev-G Extended Bowed Panels

Table 2: Windward Trip locations and fiducial marks.

Fiducial	x/L	y/L	Notes
CL1	0.0523	0	
CL2	0.0981	0	
CL3	0.1963	0	
AL3-40	0.1963	±0.0563	*P/S*
AL3-30	0.1963	±0.0712	*P/S*
AL3-20	0.1963	±0.0852	*P/S*
CL4	0.3271	0	
AL4-40	0.3271	±0.1011	*P/S*
AL4-30	0.3271	±0.1211	*P/S*
AL4-20	0.3271	±0.1377	*P/S*
CL5	0.4514	0	
FM5	0.4514	±0.1038	*P/S*
AL5-40	0.4514	±0.1446	*P/S*
AL5-40W	0.4514	±0.1554	*P/S, Wing*
AL5-30	0.4514	±0.1663	*P/S*
AL5-30W	0.4514	±0.1743	*P/S, Wing*
AL5-20	0.4514	±0.1823	*P/S*
AL5-20W	0.4514	±0.1903	*P/S, Wing*
CL6	0.6000	0	
AL6-40	0.6000	±0.1983	*P/S*
AL6-30	0.6000	±0.2203	*P/S*
AL6-20	0.6000	±0.2357	*P/S*
CL-Tail	0.9366	0	

Key to Notes: *P/S* indicates that marks were placed on both port and starboard side of centerline, *Wing* identifies attachment line locations that were selected to influence the wing leading edge.

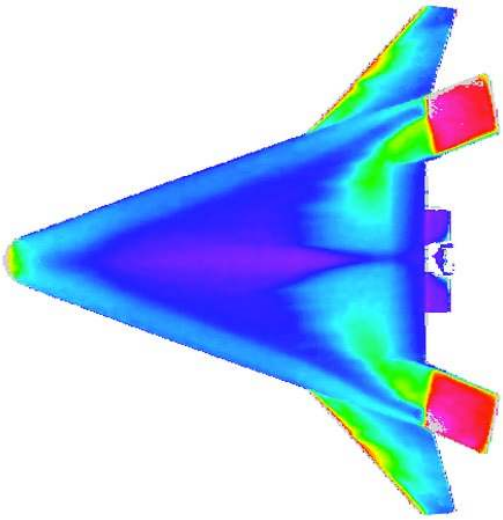

Fig 9a Effect of α on smooth body transition patterns for α = 20-deg, Re = 7.9x10^6/ft, δ_{BF} = 20-deg

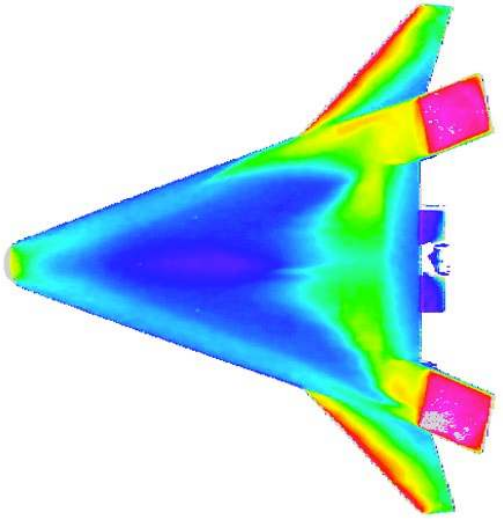

Fig 9b Effect of α on smooth body transition patterns for α = 30-deg, Re = 7.9x10^6/ft, δ_{BF} = 20-deg

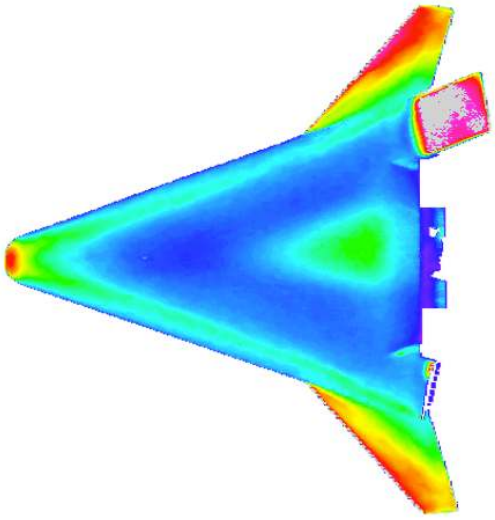

Fig 9c Effect of α on smooth body transition patterns for α = 40-deg, Re = 7.9x10^6/ft, δ_{BF} = 20-deg

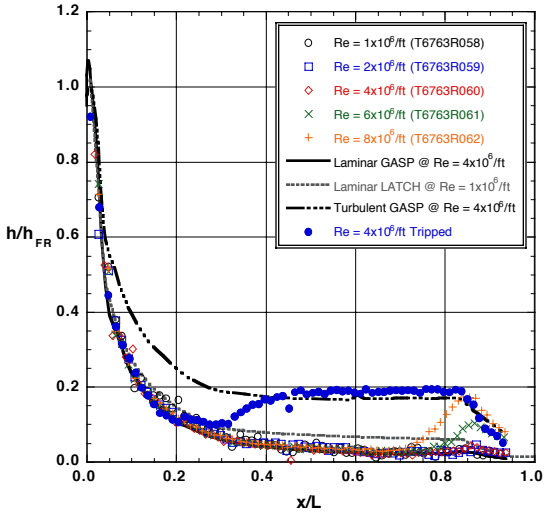

Fig 10a Effect of *Re* for smooth and tripped cases at α = 20-deg as compared to prediction

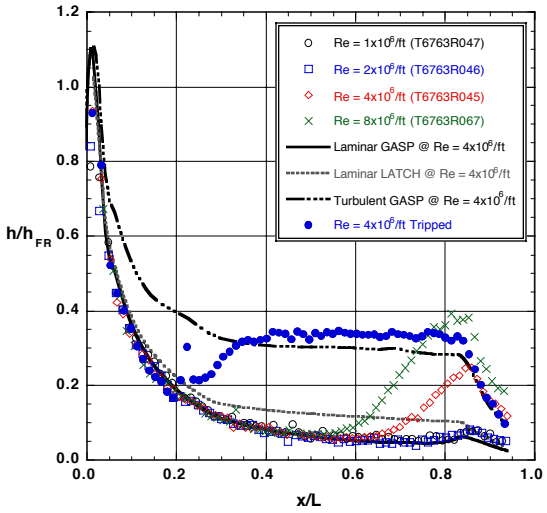

Fig 10b Effect of *Re* for smooth and tripped cases at α = 30-deg as compared to prediction

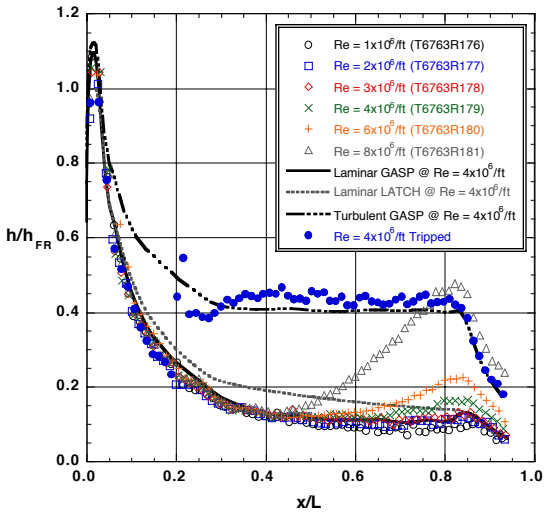

Fig 10c Effect of *Re* for smooth and tripped cases at α = 40-deg as compared to prediction

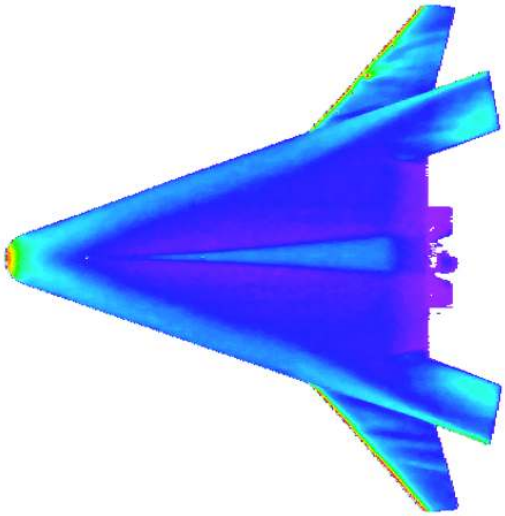

Fig 11a Effect of 0.005-in discrete trip at CL3 for α = 20-deg, Re = 4.2x10^6/ft, δ_{BF} = 0-deg

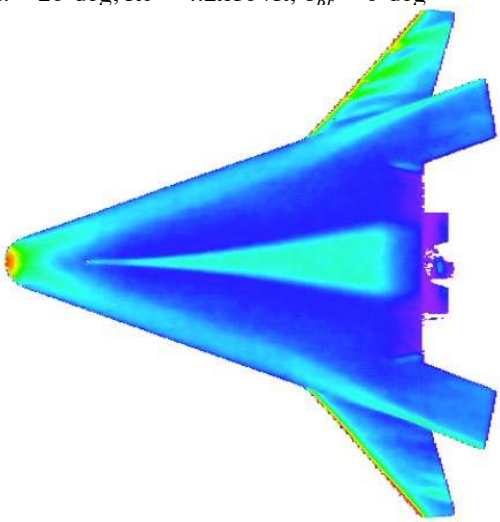

Fig 11b Effect of 0.005-in discrete trip at CL3 for α = 30-deg, Re = 4.2x10^6/ft, δ_{BF} = 0-deg

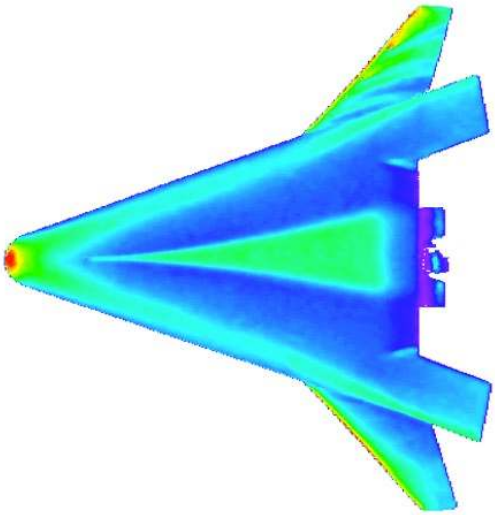

Fig 11c Effect of 0.005-in discrete trip at CL3 for α = 40-deg, Re = 3.1x10^6/ft, δ_{BF} = 0-deg

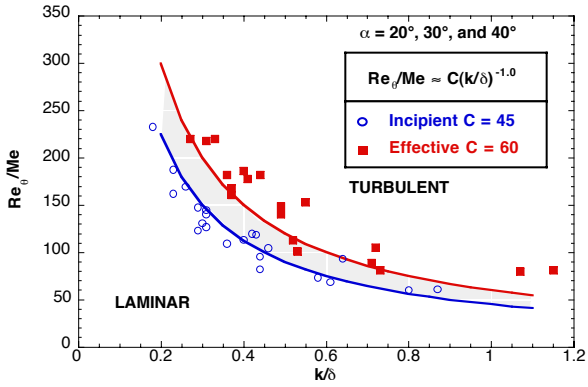

Fig 12 Results of X-33 windward centerline transition correlation

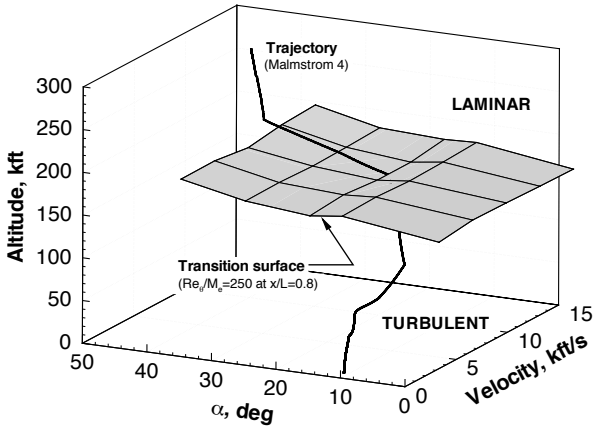

Fig 13 X-33 windward transition criterion based on Re_θ/M_e = 250 at x/L = 0.8 on centerline (Ref. 6)

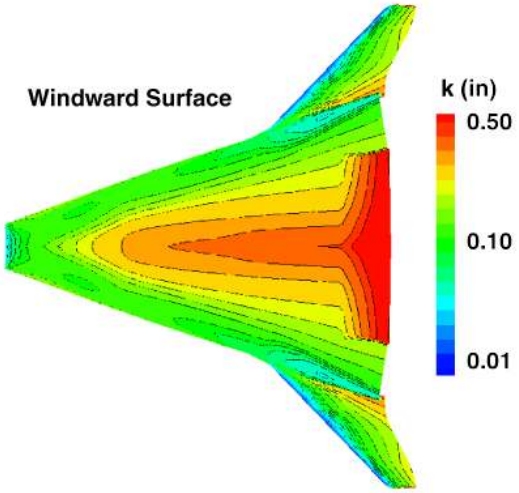

Fig 14 Allowable roughness for X-33 windward surface based on transition criterion (Ref. 6)

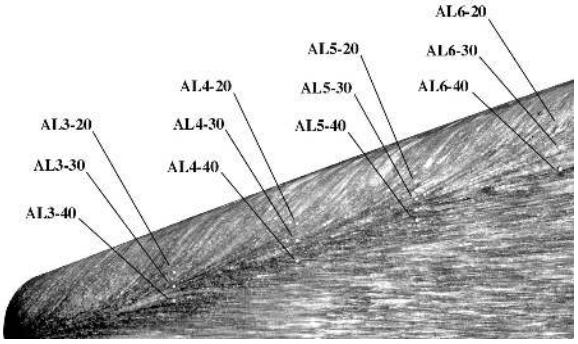

Fig 15 Surface streamlines showing attachment line location for $\alpha = 30$-deg

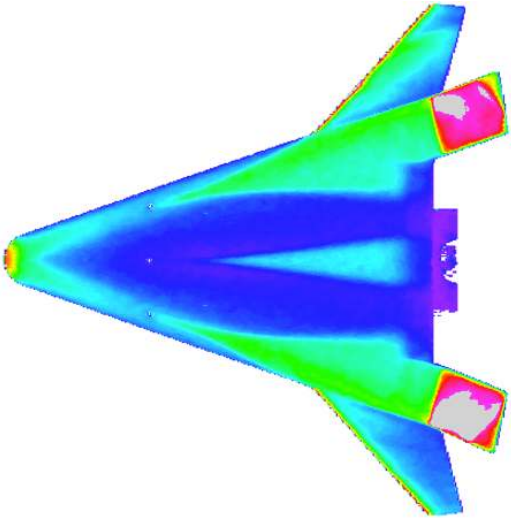

Fig 16a Effect of station-4 0.005-in trips on transition for $\alpha = 30$-deg, $Re = 3.1\text{x}10^6$/ft, $\delta_{BF} = 20$-deg

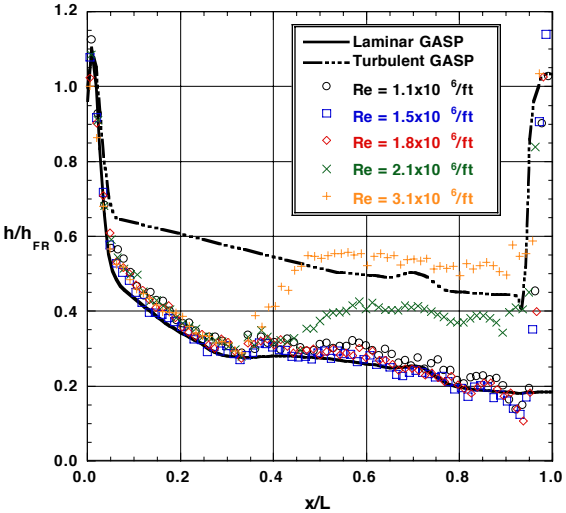

Fig 16b Effect of Re on heating along chine with 0.005-in trips at AL4-30 for $\alpha = 30$-deg

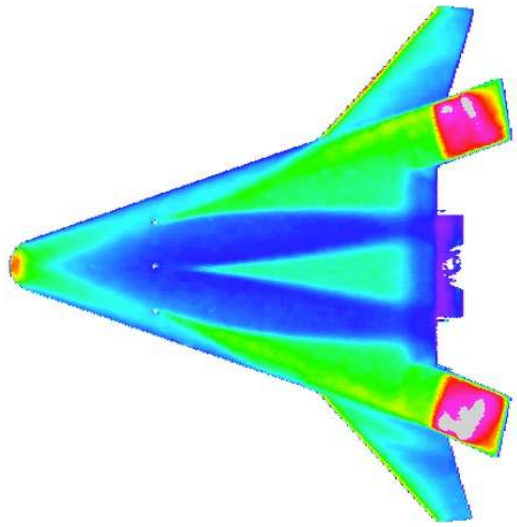

Fig 17a Effect of station-4 0.005-in trips on transition for $\alpha = 40$-deg, $Re = 3.1\text{x}10^6$/ft, $\delta_{BF} = 20$-deg

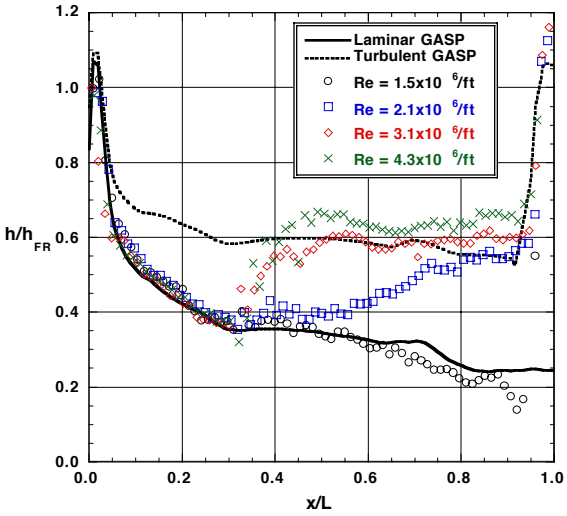

Fig 17b Effect of Re on heating along chine with 0.005-in trips at AL4-40 for $\alpha = 40$-deg

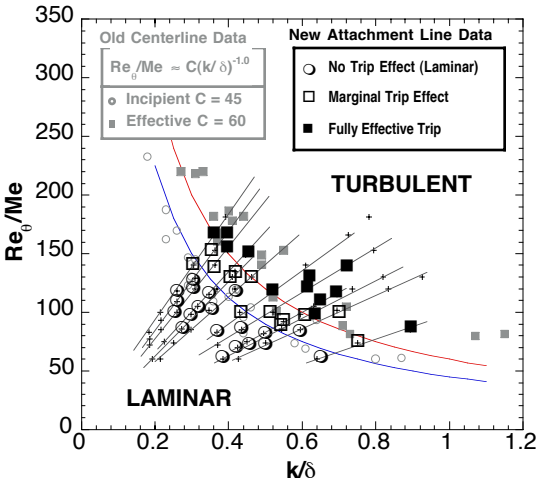

Fig 18 Attachment line results compared to previous centerline discrete roughness correlation

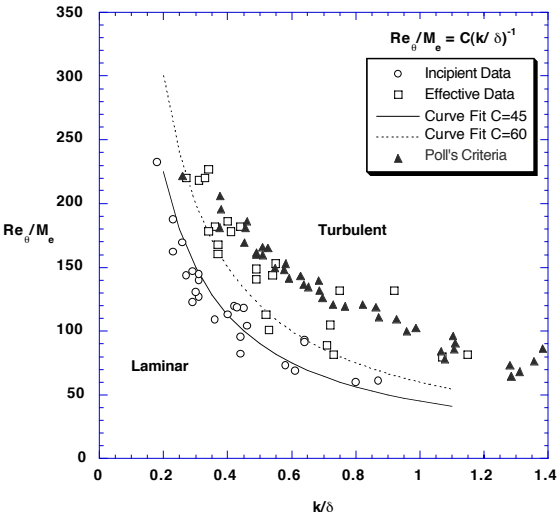

Fig 19 Comparison of X-33 roughness transition correlation to Poll's criteria (Ref. 29)

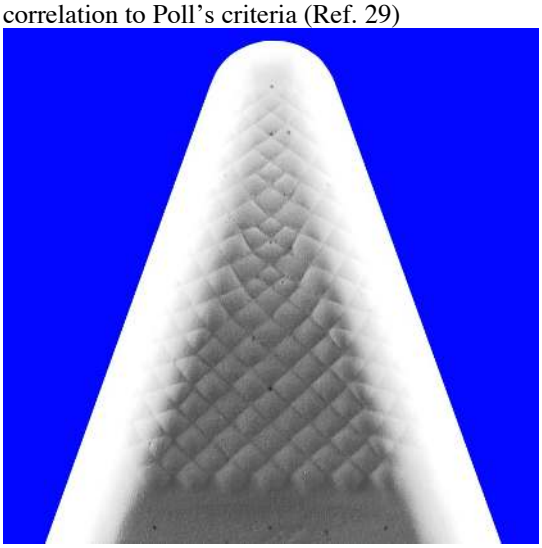

Fig 20 Photograph of k=0.008-in extended bowed panels model

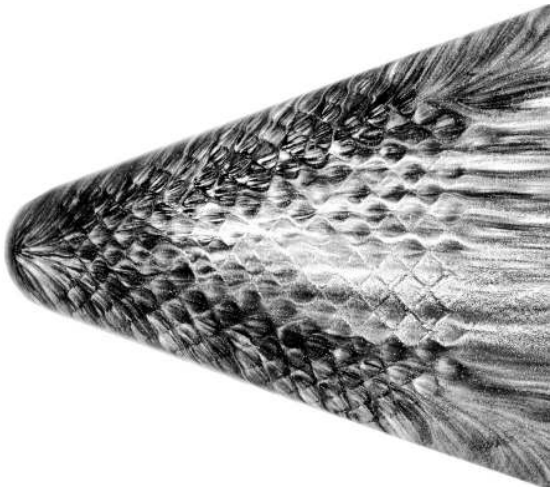

Fig 21 Close-up of streamlines around k=0.008-in extended bowed panels for α = 40-deg, Re = 2x10^6/ft

Fig 22 Effect of k=0.008-in extended bowed panels on bow shock for α = 40-deg, Re = 4x10^6/ft, δ_{BF} = 0-deg

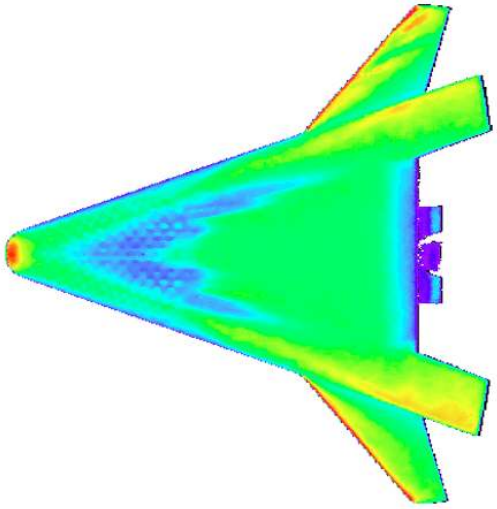

Fig 23 Effect of extended bowed panels (k=0.008-in) on heating for α = 40-deg, Re = 4x10^6/ft, δ_{BF} = 0-deg

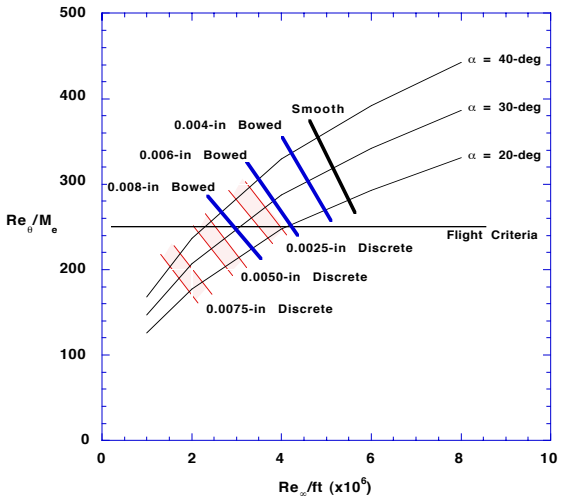

Fig 24 Comparison of wind tunnel results of smooth, bowed and discrete trip tests to flight criteria